IEEE Access
Multidisciplinary | Rapid Review | Open Access Journal

Received December 5, 2019, accepted December 16, 2019, date of publication December 25, 2019, date of current version January 7, 2020.

Digital Object Identifier 10.1109/ACCESS.2019.2962224

Drone-Initiated D2D-Aided Multihop Multicast Networks for Emergency Information Dissemination

XIAOHUI ZHOU[1], (Student Member, IEEE), SALMAN DURRANI[1], (Senior Member, IEEE), AND JING GUO[2], (Member, IEEE)

[1]Research School of Electrical, Energy and Materials Engineering, College of Engineering and Computer Science, The Australian National University, Canberra, ACT 2601, Australia
[2]School of Information and Electronics, Beijing Institute of Technology, Beijing 100081, China

Corresponding author: Jing Guo (jingguo@bit.edu.cn)

This work was supported in part by the Australian Research Council's Discovery Project Funding Scheme under Project DP170100939, in part by the National Natural Science Foundation of China under Grant 61871032, and in part by the Beijing Institute of Technology Research Fund Program for Young Scholars.

ABSTRACT Due to their fast and flexible deployment, drones can support terrestrial networks for rapid information dissemination by broadcasting emergency messages to ground devices in public safety scenarios (e.g., bushfire and flood). In this paper, we consider a drone-initiated device-to-device-aided (D2D-aided) multihop multicast network where a drone is deployed to broadcast an emergency alert message to all terrestrial D2D users at the first time slot. After that, the D2D users that have successfully received the message become the active transmitters and multicast the message through multihop for the next time slots. Using stochastic geometry, we propose a general analytical framework to compute the link coverage probability, the mean local delay for a D2D user and the network coverage probability. The Monte Carlo simulation results confirm the accuracy of the proposed framework. Our results reveal the impacts of the different system parameters (i.e., height and transmit power of the drone and density and sensitivity radius of the D2D users) on the link performance and the network performance. It is found that a higher drone altitude provides better link and network coverage probabilities and lower mean local delay. The results show that under practical setups, the cell edge user located 2 km from the ground projection of the drone has a link coverage probability around 90% after 5 time slots and a mean local delay of 2.32 time slots with a drone height as low as 200 m.

INDEX TERMS Drone communications, device-to-device (D2D) communications, stochastic geometry, emergency information dissemination.

I. INTRODUCTION

Drones have high mobility and can be easily and flexibly deployed and rapidly and dynamically reconfigured to provide on-demand wireless communication to terrestrial users. They avoid the need for highly constrained and expensive infrastructures as terrestrial base stations do. Due to the unique features of drones, a number of prospective use cases for the deployment of drones in wireless communication systems have been identified in [1]–[3]. These include important use cases for emergency scenarios, such as providing robust service between first responders and victims for search and rescue operations.

The associate editor coordinating the review of this manuscript and approving it for publication was Yougan Chen.

Natural and human-instigated disasters, such as bushfires and floods, strike many countries, such as Australia, China and USA, every year. They cause loss of life, injury, property damage and economic disruption. In unexpected public safety situations, fast, flexible and reliable emergency communication systems will not only provide ubiquitous connectivity, but can also minimize and even prevent the loss for the affected community. However, the existing terrestrial communication infrastructures can be partially or completely damaged during the disasters. Moreover, wireless network coverage may not reach all locations where mobile terminals are located, such as rural areas and forests.

In this regard, drones can be deployed to fulfill the vital need of public safety communications by broadcasting common emergency alert messages among ground terminals

to assist terrestrial networks for rapid spread of emergency information. Furthermore, device-to-device (D2D) communications is an effective technique for network coverage improvement in terrestrial communication systems by enabling direct communications between nearby mobile terminals [4]. Therefore, efficient and rapid emergency information dissemination can be achieved in public safety scenarios by exploiting both D2D communications and drone mobility. The investigation of drone-initiated D2D-aided multihop multicast networks for the rapid spread of emergency alert messages in public safety scenarios is a timely and important open problem in the literature which is addressed in this work.

A. RELATED WORK

The literature review covers four aspects related to this work: (i) use of drones for information dissemination, (ii) use of drones for coverage in wireless networks, (iii) analysis of drone communication networks using stochastic geometry and (iv) multicast transmission without assistance from drone. Generally, the papers in the first two categories use optimization techniques and have a different focus from our work. The aerial channel model adopted in this work is similar to those adopted by papers in the third category. The last category, which includes related work on D2D using stochastic geometry, is most relevant to this paper.

1) DRONE-ASSISTED NETWORK

Recently, the use of drones for information dissemination has drawn attention in the literature [5]–[9]. For instance, in [5], the authors presented an idea to use D2D communications to help a drone to achieve efficient information dissemination to a large number of ground nodes. An energy efficient data dissemination approach based on the fire fly optimization algorithm was proposed in [6] for wireless sensor networks by the use of multiple drones. Optimal transmission strategy for data dissemination was investigated in [7] to maximize the network throughput of a cooperative drone assisted vehicular ad hoc networks (VANETs) while guarantee the delay constraint. In [8], the authors studied the data dissemination problem in VANETs with assistance of drones as relay nodes. The recursive least squares algorithm and the maximum vehicle coverage algorithm were proposed to maximize the system throughput and minimize the transmission delay. An analytical model for finding the optimal height and antenna beamwidth of a drone was provided in [9] to maximize the throughput in downlink multicasting, downlink broadcasting and uplink multiple access cases.

Different from information dissemination, many papers have investigated the use of drones to provide downlink coverage in wireless networks. To maximize the minimum rate of ground users served by drone, [10] investigated the joint user scheduling and drone trajectory optimization and a model with drone employing non-orthogonal multiple access was studied in [11]. The optimal placement of a drone was found in [12] to maximize the number of covered users by the aerial base station. A mobility control algorithm was proposed in [13] for multiple mobile drones to serve moving ground devices. Some papers evaluated the drone communication networks using stochastic geometry. Specifically, the performance of cluster based drones to provide coverage after disaster was studied in [14]. In [15], the authors studied the coverage and rate of ground users served by a single static drone and a single mobile drone with underlay D2D users. The work in [16] provided the downlink performance analysis for a finite network formed by multiple drones, while [17] studied the downlink coverage probability of multiple directional beamforming drones. The coverage performance of drone wireless networks by considering three path-loss models with different line-of-sight (LOS) probability functions was investigated in [18]. In [19], the authors analyzed the downlink coverage probability of multiple drones in an urban environment. The coverage and rate in a Poisson field of drone base stations was studied in [20]. Other works have also looked at drone used as relay and its location optimization problems [21]–[23].

2) MULTICAST NETWORK

There are also some previous works on multicast transmission without assistance from drone [24]–[29]. For example, the time and the average energy consumption of serving a content request via D2D unicast and multicast content delivery were investigated in [24]. In [25], the joint optimization of power control and channel allocations was studied to maximize the aggregate rate of a cellular network with unicast cellular users and underlay multicast D2D users. In [26], the authors analyzed the coverage probability, the mean number of covered receivers (RXs) and the throughput of a multicast D2D network with and without the help from overlay cellular networks using stochastic geometry and explored how to improve the network performance by optimizing the multicast rate and the number of retransmission times. Note that the formulation in [26] cannot be directly applied to our scenario because it studied the spatially averaged performance and did not account for how the performance is evolving with different time slots through multihop. The capacity gains from two-hop cooperative multicasting was first analyzed in [27] for ad hoc networks. The paper proposed a new metric, network scaling exponent, to measure the rate of decrease of outage probability with network size. The average multicast rate and the outage rate of small-scale two-hop D2D multicast networks were studied in [28]. In [29], the authors investigated the multicast transmission capacity of single-hop and multihop multicast ad hoc networks. However, the multihop scheme considered in [29] is different from the one in this paper. For the multihop scheme in [29], each multicast cluster was considered to tessellate into smaller multicast regions of equal area. A packet was assumed to deliver slot by slot from one region to the next until all the tessellated regions have been visited by the packet.

B. CONTRIBUTIONS

In this work, we explore the use of a drone for emergency information dissemination in a public safety scenario.

We consider a drone-initiated D2D-aided multihop multicast network where a drone is deployed to broadcast an emergency alert message to all terrestrial D2D users at the first time slot. After that, the D2D users that have successfully received the message become the active transmitters (TXs) for the next time slots to multicast the emergency alert message through multihop. The main contributions and findings of this paper are summarized as follows:

- Using stochastic geometry, we develop a general analytical framework to compute the link coverage probability, the mean local delay for a D2D user and the network coverage probability. For tractable analysis, we propose an approximation for the network coverage probability. The simulation results verify the accuracy of the proposed framework.
- Based on our proposed models, we analyze the effect of the different system parameters (i.e., height and transmit power of the drone and density and sensitivity radius of the D2D users) on the link coverage probability, the mean local delay of a D2D user and the network coverage probability.
- Our results demonstrate that a higher drone altitude provides better link and network coverage probabilities and lower mean local delay. Under practical setups, the cell edge user located 2 km from the ground projection of the drone has a link coverage probability around 90% after 5 time slots and a mean local delay of 2.32 time slots with a drone altitude as low as 200 m.

C. NOTATION AND PAPER ORGANIZATION

The following notation is used in this paper. $\Pr(\cdot)$ indicates the probability measure and $\mathbb{E}[\cdot]$ denotes the expectation operator. j is the imaginary number and $\mathrm{Re}[\cdot]$ denotes the real part of a complex number. $|\cdot|$ is the Lebesgue measure, which is the area in a two-dimensional case.
$\Gamma(x) = \int_0^\infty t^{x-1}\exp(-t)\mathrm{d}t$ is the complete Gamma function.
${}_2F_1(a,b;c;z) = \frac{\Gamma(c)}{\Gamma(b)\Gamma(c-b)}\int_0^1 \frac{t^{b-1}(1-t)^{c-b-1}}{(1-tz)^a}\mathrm{d}t$ is the Gaussian hypergeometric function.
$\mathcal{L}_X(s) = \mathbb{E}[\exp(-sX)]$ denotes the Laplace transform of a random variable X.
A list of the main mathematical symbols employed in this paper is given in Table 1.

The rest of the paper is organized as follows: Section II describes the system model and assumptions. Section III focuses on the link performance of a D2D user. Section IV details the analysis of the network coverage probability. Section V presents the results and the effect of the system parameters on the link performance and the network performance. Finally, Section VI concludes the paper.

II. SYSTEM MODEL

A drone-initiated D2D-aided multihop multicast network is considered in this paper, where an emergency alert message needs to be conveyed to all terrestrial D2D users under a public safety scenario. The terrestrial D2D users are assumed to be uniformly distributed over a disk network region $\mathcal{S}$ with radius R_C, i.e., $|\mathcal{S}| = \pi R_C^2$, and their locations form a Poisson point process (PPP) ϕ with density λ inside $\mathcal{S}$ and 0 otherwise. Throughout the paper, we use X_i to denote both the random location as well as the ith D2D user itself. We assume that the cellular network is unavailable or not operational, for instance, due to a natural disaster. A drone flies to the center of the network region and broadcasts an emergency alert message from a height of h, as shown in Figure 1 at the top of the next page.[1] Then the drone flies out of the network region and the terrestrial D2D users multicast the emergency alert message to each others using D2D links. For each inactive D2D user, it only receives the aggregate signal from the active D2D users residing in its sensitivity region which is generally a disk region with radius R_D centered at the inactive user.

TABLE 1. Summary of main symbols used in the paper.

Symbol	Definition
R_C	Radius of the network region
R_D	Radius of D2D sensitivity region
λ	Density of D2D users
h	Height of the drone
α_{T}	Path-loss exponent of the terrestrial link
α_{L}	Path-loss exponent of the LOS aerial link
α_{N}	Path-loss exponent of the NLOS aerial link
η_{L}	Additional attenuation factor for the LOS aerial link
η_{N}	Additional attenuation factor for the NLOS aerial link
m_{L}	Nakagami-m fading parameter for the LOS aerial link
m_{N}	Nakagami-m fading parameter for the NLOS aerial link
p_{L}	LOS probability
p_{N}	NLOS probability
P_{A}	Drone transmit power
P_{D}	Active D2D user transmit power
γ	SNR threshold
σ^2	Noise power

A. CHANNEL MODEL

It has been shown by the measurements that aerial links experience different channel characteristics comparing to terrestrial links [30]. The aerial links between the drone and the D2D users can be either LOS or non-line-of-sight (NLOS) with different probabilities of occurrence p_{L} and p_{N}, which are determined by altitude and type of the drone, elevation angle, type of propagation environment, density and height of buildings [31].

The path-loss of the NLOS aerial link is greater than the LOS one, because of the shadowing effect and the reflection of signals from obstacles. Depending on the LOS or NLOS link between the drone and the D2D user, the path-loss of the aerial link with a three-dimensional propagation distance of z is modeled as [15], [32]

$$PL_a(z) = \begin{cases} \eta_{\mathrm{L}} z^{-\alpha_{\mathrm{L}}}, & \text{LOS} \\ \eta_{\mathrm{N}} z^{-\alpha_{\mathrm{N}}}, & \text{NLOS} \end{cases}, \quad (1)$$

[1] Note that in this work we are inherently exploiting the drone mobility in seeding the common emergency alert message, since the drone can be deployed at any height h.

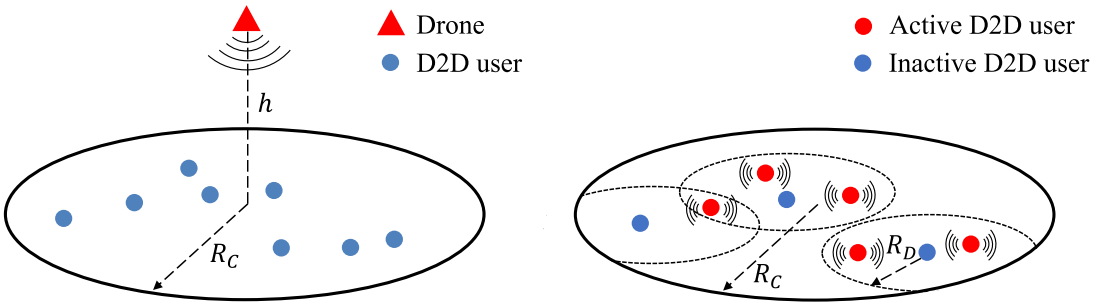

(a) First time slot T_0: Drone broadcasting.

(b) Second time slot onwards $T_n, n = 1, 2, 3 \cdots$: D2D multicasting.

FIGURE 1. Illustration of the system model.

where α_{L} and α_{N} denote the path-loss exponent of LOS aerial link and NLOS aerial link respectively. η_{L} and η_{N} is the additional attenuation factor for LOS aerial link and NLOS aerial link respectively.

As for the small-scale fading, the aerial links are assumed to experience Nakagami-m fading with different fading parameters m_{L} and m_{N} for the LOS aerial link and the NLOS aerial link respectively. The aerial links also experience additive white Gaussian noise (AWGN) with variance σ^2.

The path-loss of the terrestrial link between the D2D users with a propagation distance of ℓ is defined as $\ell^{-\alpha_{\mathrm{T}}}$, where α_{T} is the path-loss exponent. Furthermore, we assume the terrestrial links experience independent small-scale Rayleigh fading and AWGN with variance σ^2.

B. TRANSMISSION MODEL

For the considered multihop multicast transmission scheme, time is slotted and the emergency alert message is delivered using multiple time slots to the D2D users on the ground through two phases.

1) DRONE BROADCASTING PHASE

In the first time slot T_0, the drone broadcasts an emergency alert message to all terrestrial D2D users. At the end of the first time slot, terrestrial D2D users attempt to decode the message. User X_i decodes successfully if and only if the received signal-to-noise ratio (SNR) is greater than a threshold γ. The instantaneous SNR at the D2D user at the first time slot T_0 is given as

$$\mathsf{SNR}_0 = \frac{P_{\mathrm{A}} G PL_a(\mathcal{Z})}{\sigma^2}, \tag{2}$$

where P_{A} is the transmit power of the drone. G is the aerial link fading power gain, which follows Gamma distribution. $\mathcal{Z}$ is the Euclidean distance between the drone and the terrestrial D2D user. The path-loss of the aerial link $PL_a(\cdot)$ is given in (1).

2) D2D MULTICASTING PHASE

From the second time slot onwards, all D2D users that have successfully received the emergency alert message in the previous time slot become the active TXs and multicast the common message for the current time slot. Since the emergency alert message is a common message for all the terrestrial D2D users, there is no mutual interference between the D2D transmissions. The inactive D2D user is able to receive the aggregate signal from all the active neighbor D2D TXs within its sensitivity region with radius R_D. As before, user X_j decodes the non-coherent sum of message successfully and becomes active at the end of the current time slot if the received SNR is above the threshold γ. The delivery of the emergency alert message by the multihop multicast scheme is carried out by all the active D2D users through multiple time slots (for time slots $T_n, n \neq 0$). Note that an inactive D2D user which does not decode the emergency alert message successfully in a particular time slot keeps trying to decode the message in the next time slots. Furthermore, we assume that mutual synchronization among the terrestrial D2D users is achieved by distributed synchronization algorithm and the terrestrial D2D users are static during the whole transmission [33]–[35].

SNR is an important measure that affects the state of the D2D user, whether being active (acting as a TX) or inactive (acting as a RX). For the considered setup, the instantaneous SNR at the inactive D2D user at the later time slots $T_n, n \neq 0$ is shown as

$$\mathsf{SNR}_n = \frac{P_{\mathrm{D}} \sum_{X_i \in \phi_{\mathrm{active}}} H_i \ell_i^{-\alpha_{\mathrm{T}}}}{\sigma^2}, \quad n \neq 0, \tag{3}$$

where P_{D} is the transmit power of the active D2D users. H_i is the fading power gain between the inactive D2D user and the ith active D2D TX within its sensitivity region, which follows exponential distribution. The fading power gain H_i is assumed to be independent during successive time slots. ℓ_i is the Euclidean distance between the inactive D2D user and the ith active D2D TX within its sensitivity region.

III. LINK PERFORMANCE

In this section, we provide the mathematical formulations to analyze the link performance at the given D2D user, which incorporate the analysis of both phases. We are interested in the following two performance metrics that directly reflect the perceived experience of D2D users:

- *Link coverage probability after time slot T_n, $\mathbb{P}^n_{\mathrm{cov}}(X_i)$:* The link coverage probability after time slot T_n measures

the probability that the specific D2D user X_i has successfully received the message after the given time slot.

- *Mean local delay, $\overline{D}(X_i)$:* The local delay is defined as the number of transmission attempts needed until the first success of message transmission. The mean local delay characterizes that the specific D2D user X_i successfully receives the message after $\overline{D}(X_i)$ time slots on average.

Before calculating these two metrics, we need to first look at the link success probability at each time slot which is defined as follows:

Definition 1: The link success probability at time slot T_n is the probability that the received SNR at the D2D user X_i is higher than the threshold γ. It can be expressed as

$$\mathbb{P}_s^n(X_i) \triangleq \Pr(\mathsf{SNR}_n > \gamma). \tag{4}$$

Theorem 1: Based on the system model in Section II, the link success probability at the first time slot T_0 is given as

$$\mathbb{P}_s^0(X_i) = \sum_{i=0}^{m_{\mathrm{L}}-1} \frac{p_{\mathrm{L}}}{i!} V_L^i(z_i) \exp\left(-V_L(z_i)\right) + \sum_{j=0}^{m_{\mathrm{N}}-1} \frac{p_{\mathrm{N}}}{j!} V_N^j(z_i) \exp\left(-V_N(z_i)\right), \tag{5}$$

where $V_q(z) = \frac{m_q \gamma \sigma^2 z^{\alpha_q}}{P_{\mathrm{A}} \eta_q}$, $q \in \{\mathrm{L}, \mathrm{N}\}$ and $z_i = \sqrt{X_i^2 + h^2}$.

Proof: See Appendix A. ∎

After the first time slot T_0, the drone leaves the network region and all D2D users that have successfully received the emergency alert message become the TXs and multicast the message. However, the network will be in outage if none of the D2D users has successfully received the message from the drone at the first time slot T_0.

Theorem 2: Based on the system model in Section II, the network outage probability at the first time slot T_0 is given as

$$\mathbb{P}_{\mathrm{out}} = \exp\left(-\int_h^{\sqrt{R_C^2+h^2}} 2\pi\lambda z \sum_{i=0}^{m_{\mathrm{L}}-1} \frac{p_{\mathrm{L}}}{i!} V_L^i(z) \exp(-V_L(z))\, \mathrm{d}z - \int_h^{\sqrt{R_C^2+h^2}} 2\pi\lambda z \sum_{j=0}^{m_{\mathrm{N}}-1} \frac{p_{\mathrm{N}}}{j!} V_N^j(z) \exp(-V_N(z))\, \mathrm{d}z \right). \tag{6}$$

Proof: The network will be in outage if none of the D2D users has successfully received the message from the drone at the first time slot T_0. From Theorem 1, we have

$$\mathbb{P}_{\mathrm{out}} = \mathbb{E}_\phi \left[\prod_{x\in\phi} \left(1 - \mathbb{P}_s^0(x)\right) \right] = \exp\left(-\int_0^{R_C} \mathbb{P}_s^0(x) 2\pi\lambda x \mathrm{d}x \right) \tag{7a}$$

$$= \exp\left(-\int_h^{\sqrt{R_C^2+h^2}} \mathbb{P}_s^0\left(\sqrt{z^2-h^2}\right) 2\pi\lambda z \mathrm{d}z \right), \tag{7b}$$

where (7a) follows from the probability generating functional for PPP. Substituting (5) into (7b), we can arrive at Theorem 2. ∎

Now let us assume there is at least one active D2D user broadcasting the message at time slot T_n for $n \neq 0$, the inactive D2D user receives the message from all the active TXs within its sensitivity region. The following remark discusses the challenges and proposes solution for modeling the locations of the active D2D TXs.

Remark 1: After the first time slot T_0, the positions of the active TXs within the sensitivity region of a D2D user X_i are inhomogeneous. Their distribution changes with different time slots. Moreover, the locations of the active TXs at the current time slot is correlated with their locations in the previous time slots. However, it is very difficult to provide an exact model for the location of the active TXs inside the sensitivity region. Hence, for analytical tractability, we propose to model the locations of the active TXs as independently and uniformly distributed inside the D2D user X_i's sensitivity region at time slot T_n. Note that independency refers to that the *number of active TXs inside a D2D user's sensitivity region* is independent of the *number of active TXs inside another D2D user's sensitivity region.* At time slot T_1, the active TXs inside the D2D user X_i's sensitivity region have a density of $\lambda_i^1 = \mathbb{P}_s^0(X_i)\lambda$. The density of the D2D users which are not active at T_1, but become active after T_1 is $\mathbb{P}_s^1(X_i)(1-\mathbb{P}_{\mathrm{out}})(1-\mathbb{P}_s^0(X_i))\lambda$. The active D2D TXs, including the D2D TXs that are active at time slot T_1 and the D2D TXs that become active after T_1, will jointly transmit the message to user X_i at time slot T_2. Therefore, the accumulated density of the active TXs inside the D2D user X_i's sensitivity region at time slot T_n for $n = 2, 3, 4\ldots$ is $\lambda_i^n = (\mathbb{P}_s^0(X_i) + \sum_{k=1}^{n-1} \mathbb{P}_s^k(X_i)(1 - \mathbb{P}_{\mathrm{out}}) \prod_{l=0}^{k-1}(1-\mathbb{P}_s^l(X_i)))\lambda$. The accuracy of this approximation will be validated in Section V by comparison with simulation results which is generated based on the exact system scenario rather than the approximated spatial model adopted in the analysis.

In this work, we adopt a numerical inversion method, which is easy to compute and also provides controllable error estimation [36], [37]. By numerically inverting the Laplace transform of the aggregate received signal power via a trapezoidal summation, we can express the link success probability of D2D user X_i at time slot T_n for $n \neq 0$ as below

$$\mathbb{P}_s^n(X_i) = 1 - \frac{P_{\mathrm{D}} \exp(\frac{A}{2})}{2^B \gamma \sigma^2} \sum_{b=0}^{B} \binom{B}{b} \sum_{c=0}^{C+b} \frac{(-1)^c}{D_c} \mathrm{Re}\left[\frac{\mathcal{L}_{P_i^n}(s)}{s} \right], \tag{8}$$

where $\mathrm{Re}[\cdot]$ is the real part operator, $s = \frac{(A+j2\pi c)P_{\mathrm{D}}}{2\gamma\sigma^2}$, $\mathcal{L}_{P_i^n}(s)$ is the Laplace transform of the aggregate received signal power at the user X_i, $P_i^n = \sum_{X_j \in \phi_{\mathrm{active}}} H_j \ell_j^{-\alpha_{\mathrm{T}}}$, $D_c = 2$ (if $c = 0$) and $D_c = 1$ (if $c = 1, 2, \ldots, C + b$). A, B and C are positive parameters used to control the estimation accuracy.

From (8), the key parameter in order to obtain the link success probability at time slot T_n for D2D user X_i is $\mathcal{L}_{P_i^n}(s)$. By the definition of Laplace transform of a random variable, we can express $\mathcal{L}_{P_i^n}(s)$ in the following theorem.

Theorem 3: Following the system model in Section II, the Laplace transform of the aggregate received signal power at the D2D user X_i from all the active TXs inside its sensitivity region is given as (9) at the bottom of this page, where ${}_2F_1(\cdot,\cdot;\cdot;\cdot)$ is the Gaussian (or ordinary) hypergeometric function.

Proof: See Appendix B. ∎

Although the Laplace transform of the aggregate received signal power at the D2D user X_i for $R_C - R_D < X_i \leqslant R_C$ cannot be expressed in close-form due to complexity of the inverse trigonometric functions which is inside the integration. However, it can be easily evaluated numerically using Mathematica.

Recall that the link coverage probability after time slot T_n, $\mathbb{P}^n_{\text{cov}}(X_i)$ is defined as the probability that the D2D user X_i has successfully received the message after $n+1$ time slots, which is shown as follows:

Proposition 1: Based on the system model in Section II and the definition of the link coverage probability after time slot T_n, we have

$$\mathbb{P}^n_{\text{cov}}(X_i) = \begin{cases} \mathbb{P}^0_s(X_i), & n=0 \\ \mathbb{P}^0_s(X_i) + \sum_{k=1}^{n} \mathbb{P}^k_s(X_i)(1-\mathbb{P}_{\text{out}}) & \\ \times \prod_{l=0}^{k-1}(1-\mathbb{P}^l_s(X_i)), & n=1,2,3\ldots \end{cases}, \quad (10)$$

where $\mathbb{P}^0_s(X_i)$ is given in Theorem 1 and $\mathbb{P}^k_s(X_i)$ for $k \neq 0$ is given in (8). $\mathbb{P}_{\text{out}}$ is shown in Theorem 2.

We now turn to the delay metric. For the considered drone-initiated D2D-aided multihop multicast network, the local delay at the D2D user X_i is a discrete random variable with a probability mass function as follows:

$$\Pr(D(X_i)=d) = \begin{cases} \mathbb{P}^0_s(X_i), & d=1 \\ \mathbb{P}^{d-1}_s(X_i)(1-\mathbb{P}_{\text{out}}) & \\ \times \prod_{l=0}^{d-2}(1-\mathbb{P}^l_s(X_i)), & d=2,3,4\ldots \end{cases}. \quad (11)$$

Hence the mean local delay is given by $\overline{D}(X_i) = \mathbb{E}[D(X_i)] = \sum_{d=1}^{\infty} d\Pr(D(X_i) = d)$ and the specific expression of the mean local delay is shown in the following proposition.

Proposition 2: Based on the system model in Section II, the mean local delay at the D2D user X_i is given as

$$\overline{D}(X_i) = \mathbb{P}^0_s(X_i) + \sum_{d=2}^{\infty} d\,\mathbb{P}^{d-1}_s(X_i)(1-\mathbb{P}_{\text{out}}) \prod_{l=0}^{d-2}(1-\mathbb{P}^l_s(X_i)), \quad (12)$$

where $\mathbb{P}^0_s(X_i)$ is given in Theorem 1 and $\mathbb{P}^n_s(X_i)$ for $n \neq 0$ is given in (8). $\mathbb{P}_{\text{out}}$ is shown in Theorem 2.

IV. NETWORK PERFORMANCE

In the previous section, we have focused on the link performance where the distance between the D2D user and the ground projection of the drone is known. Now we turn to study the network performance charaterized by the network coverage probability after time slot T_n. $\mathbb{P}^n_{\text{cov}}$ measures the average probability that a randomly chosen D2D user in the network has successfully received the message after time slot T_n, in other words, it presents the fraction of active D2D TXs in the network after the given time slot.

Before looking into the network coverage probability, we first investigate the network success probability at time slot T_n. To evaluate the network success probability, we need to calculate the expectancy of the link success probability over the spatial distribution of the distance between a D2D user and the ground projection of the drone. The expression of the network success probability is given as (13) at the bottom of this page, where $s = \frac{(A+j2\pi c)P_{\text{D}}}{2\gamma\sigma^2}$, the Laplace transform of the aggregate received signal power $\mathcal{L}_{P^n_i}(s)$ is given in Theorem 3, $D_c = 2$ (if $c = 0$) and $D_c = 1$ (if $c = 1, 2, \ldots, C+b$).

Remark 2: To the best of our knowledge, it is not easy to evaluate the integration $\int_h^{\sqrt{R_C^2+h^2}} \frac{2z}{sR_C^2}\mathcal{L}_{P^n_i}(s)\text{d}z$ due to the non-closed-form Laplace transform. We propose to make a simplification assumption that, from the second time slot onwards, a D2D user will become active if there is one or more active TXs multicasting the message within its sensitivity region. We show that this approximation allows tractable

$$\mathcal{L}_{P^n_i}(s) = \begin{cases} \exp\left(-\pi\lambda^n_i R_D^2 + \pi\lambda^n_i R_D^{2+\alpha_{\text{T}}} \frac{2}{s(\alpha_{\text{T}}+2)}\,{}_2F_1\left(1, 1+\frac{2}{\alpha_{\text{T}}}; 2+\frac{2}{\alpha_{\text{T}}}; -\frac{R_D^{\alpha_{\text{T}}}}{s}\right)\right), & X_i \leqslant R_C - R_D \\ \exp\left(-\pi\lambda^n_i (R_C - X_i)^2 \left(1 - \frac{2(R_C-X_i)^{\alpha_{\text{T}}}}{s(\alpha_{\text{T}}+2)}\,{}_2F_1\left(1, 1+\frac{2}{\alpha_{\text{T}}}; 2+\frac{2}{\alpha_{\text{T}}}; -\frac{(R_C-X_i)^{\alpha_{\text{T}}}}{s}\right)\right)\right) & \\ \times \exp\left(-\int_{R_C-X_i}^{R_D} \frac{2s\lambda^n_i \ell}{\ell^{\alpha_{\text{T}}}+s} \text{arcsec}\left(\frac{2\ell X_i}{\ell^2 + X_i^2 - R_C^2}\right)\text{d}\ell\right), & R_C - R_D < X_i \leqslant R_C \end{cases}. \quad (9)$$

$$\mathbb{P}^n_s = \begin{cases} \int_h^{\sqrt{R_C^2+h^2}} \frac{2z}{R_C^2} \sum_{i=0}^{m_{\text{L}}-1} \frac{p_{\text{L}}}{i!} V_L^i(z)\exp\left(-V_L(z)\right)\text{d}z + \int_h^{\sqrt{R_C^2+h^2}} \frac{2z}{R_C^2} \sum_{j=0}^{m_{\text{N}}-1} \frac{p_{\text{N}}}{j!} V_N^j(z)\exp\left(-V_N(z)\right)\text{d}z, & n=0 \\ 1 - \frac{P_{\text{D}}\exp\left(\frac{A}{2}\right)}{2^B\gamma\sigma^2} \sum_{b=0}^{B}\binom{B}{b}\sum_{c=0}^{C+b}\frac{(-1)^c}{D_c}\text{Re}\left[\int_h^{\sqrt{R_C^2+h^2}} \frac{2z}{sR_C^2}\mathcal{L}_{P^n_i}(s)\text{d}z\right], & n=1,2,3\ldots \end{cases}. \quad (13)$$

computation of the network success probability at time slot T_n for $n \neq 0$. Our results in Section V show that a good level of accuracy is obtained with this approximation.

Lemma 1: Following the system model in Section II, the approximated link success probability for D2D user X_i at time slot T_n for $n = 1, 2, 3 \ldots$ is given as (14) at the bottom of this page, where

$$\lambda_i^n = (\mathbb{P}_s^0(X_i) + \sum_{k=1}^{n-1} \widetilde{\mathbb{P}}_s^k(X_i)(1 - \mathbb{P}_{\text{out}}) \prod_{l=0}^{k-1} (1 - \widetilde{\mathbb{P}}_s^l(X_i)))\lambda.$$

Proof: See Appendix C. ∎

Using the approximated link success probability above, we can express the approximated network success probability at time slot T_n for $n = 1, 2, 3 \ldots$ as (15) shown at the bottom of this page, where

$$\lambda_i^n = (\mathbb{P}_s^0(X_i) + \sum_{k=1}^{n-1} \widetilde{\mathbb{P}}_s^k(X_i)(1 - \mathbb{P}_{\text{out}}) \prod_{l=0}^{k-1} (1 - \widetilde{\mathbb{P}}_s^l(X_i)))\lambda.$$

Proposition 3: Based on the system model in Section II, the network coverage probability after time slot T_n is given as

$$\mathbb{P}_{\text{cov}}^n = \begin{cases} \mathbb{P}_s^0, & n = 0 \\ \mathbb{P}_s^0 + \widetilde{\mathbb{P}}_s^1(1-\mathbb{P}_{\text{out}})(1-\mathbb{P}_s^0), & n = 1 \\ \mathbb{P}_s^0 + \widetilde{\mathbb{P}}_s^1(1-\mathbb{P}_{\text{out}})(1-\mathbb{P}_s^0) & \\ + \sum_{k=2}^{n} \widetilde{\mathbb{P}}_s^k(1-\mathbb{P}_{\text{out}}) & \\ \quad \times (1-\mathbb{P}_s^0) \prod_{l=1}^{k-1} (1-\widetilde{\mathbb{P}}_s^l), & n = 2, 3 \ldots \end{cases}, \quad (16)$$

where $\mathbb{P}_s^0$ is given in (13) and $\widetilde{\mathbb{P}}_s^k$ is given in (15). $\mathbb{P}_{\text{out}}$ is shown in Theorem 2.

The key performance metrics are summarized in Table 2.

V. RESULTS

In this section, we first validate the analytical results of both the link performance and the network performance and then discuss the design insights of a drone-initiated D2D-aided multihop multicast network. The simulation results are obtained using system level computer simulations in Matlab

TABLE 2. Summary of the analytical model for drone-initiated D2D-aided multihop multicast networks.

Performance metrics	General form	Key factor(s)
Link coverage probability	Proposition 1	$\mathbb{P}_s^0(X_i)$ in (5) $\mathbb{P}_{\text{out}}$ in (6) $\mathbb{P}_s^n(X_i)$ for $n \neq 0$ in (8)
Mean local delay	Proposition 2	$\mathbb{P}_s^0(X_i)$ in (5) $\mathbb{P}_{\text{out}}$ in (6) $\mathbb{P}_s^n(X_i)$ for $n \neq 0$ in (8)
Network coverage probability	Proposition 3	$\mathbb{P}_{\text{out}}$ in (6) $\mathbb{P}_s^0$ in (13) $\widetilde{\mathbb{P}}_s^n$ in (15)

TABLE 3. Parameter values.

Parameter	Value	Parameter	Value
R_D	75 m	α_{T}	4
R_C	2000 m	α_{L}	2.5
h	200 m	α_{N}	4
λ	50 /km^2	η_{L}	0 dB
γ	0 dBm	η_{N}	-20 dB
P_{A}	25 dBm	m_{L}	5
P_{D}	10 dBm	m_{N}	1
σ^2	-100 dBm		

based on the exact system scenario by averaging over 10^6 Monte Carlo simulation runs. We set $A = 24$, $B = 20$ and $C = 30$ in order to achieve an estimation error of 10^{-10}. Unless stated otherwise, the values of the other parameters summarized in Table 3 are used. We set the values of α_{L}, α_{N}, η_{L}, η_{N}, m_{L} and m_{N} for urban environment. Note that the probability for local delay greater than 50 time slots is very small and negligible under the considered system parameters, so we only sum up from $d = 2$ to $d = 50$ in the calculation of the mean local delay in Proposition 2 for the results presented in this section.

To generate the results in this section, we adopt a widely used aerial channel model [31], [38], [39]. The LOS probability is given as $p_{\text{L}} = \frac{1}{1+C_a \exp\left(-B_a\left[\frac{180}{\pi}\sin^{-1}\left(\frac{h}{z}\right)-C_a\right]\right)}$ and the NLOS probability is $p_{\text{N}} = 1 - p_{\text{L}}$. $C_a = 9.6117$ and $B_a = 0.1581$ for signal transmission in an urban environment.

A. LINK COVERAGE PROBABILITY

Figure 2(a) and Figure 2(b) plot the link coverage probability of a D2D user after the first time slot T_0, $\mathbb{P}_{\text{cov}}^0(X_i)$, and after

$$\widetilde{\mathbb{P}}_s^n(X_i) = \begin{cases} 1 - \exp(-\lambda_i^n R_D^2 \pi), & X_i \leqslant R_C - R_D \\ 1 - \exp\left(\lambda_i^n R_D^2 \left(\arccos\left(\frac{R_C^2 - X_i^2 - R_D^2}{2X_i R_D}\right) - \pi\right) - \lambda_i^n R_C^2 \arccos\left(\frac{R_C^2 + X_i^2 - R_D^2}{2X_i R_C}\right)\right) & \\ \times \exp\left(\frac{\lambda_i^n}{2}\sqrt{-R_C^4 - R_D^4 - X_i^4 + 2R_C^2X_i^2 + 2R_D^2X_i^2 + 2R_C^2R_D^2}\right), & R_C - R_D < X_i \leqslant R_C \end{cases}. \quad (14)$$

$$\widetilde{\mathbb{P}}_s^n = \int_0^{R_C - R_D} \frac{2x}{R_C^2} - \frac{2x}{R_C^2} \exp(-\lambda_i^n R_D^2 \pi) \mathrm{d}x + \int_{R_C - R_D}^{R_C} \frac{2x}{R_C^2} \left(1 - \exp\left(\lambda_i^n R_D^2 \left(\arccos\left(\frac{R_C^2 - x^2 - R_D^2}{2xR_D}\right) - \pi\right)\right.\right.$$
$$\left.\left. - \lambda_i^n R_C^2 \arccos\left(\frac{R_C^2 + x^2 - R_D^2}{2xR_C}\right) + \frac{\lambda_i^n}{2}\sqrt{-R_C^4 - R_D^4 - x^4 + 2R_C^2x^2 + 2R_D^2x^2 + 2R_C^2R_D^2}\right)\right) \mathrm{d}x. \quad (15)$$

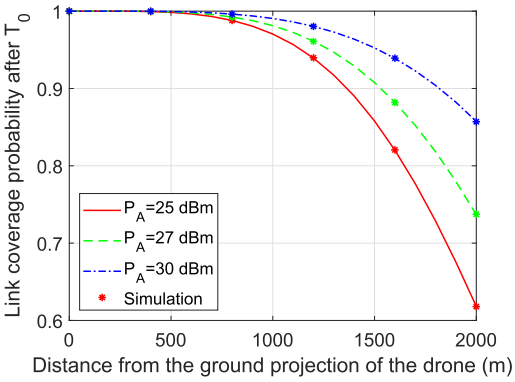

(a) Link coverage probability after the first time slot T_0 with different transmit power of the drone and simulations.

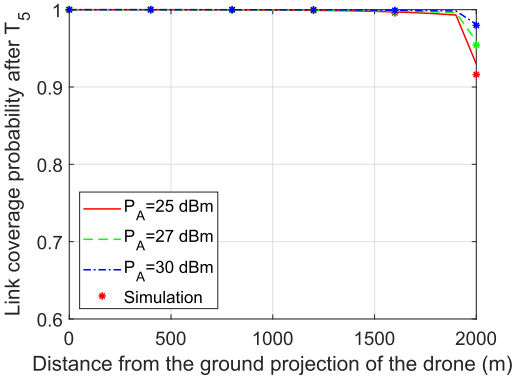

(b) Link coverage probability after time slot T_5 with different transmit power of the drone and simulations.

FIGURE 2. Link coverage probabilities versus the distance of D2D user from the ground projection of the drone with simulations.

time slot T_5, $\mathbb{P}^5_{\text{cov}}(X_i)$, against its distance from the ground projection of the drone with different transmit power of the drone respectively. The analytical results are obtained using Proposition 1. For both link coverage probabilities, the simulation results match very well with the analytical results with the maximum value of the relative absolute error, defined as $\frac{|\text{simulation value}-\text{analytical value}|}{\text{simulation value}}$, less than 1.5%. This validates the accuracy of our analytical framework.

From Figure 2(b), we can see that the link coverage probability at the D2D user close to the ground projection of the drone is very closed to 1 after time slot T_5. Therefore, we focus on the link coverage probability at the cell edge D2D user, i.e., user located at 2 km from the ground projection of the drone. In the results presented later in this work, we investigate the effect of some important system parameters, the transmit power and the height of the drone and the density and the sensitivity radius of the D2D users, on the link coverage probability of the cell edge user.

B. IMPACT OF DRONE TRANSMIT POWER

Figure 3(a) plots the link coverage probability after time slot T_n at the cell edge user located at 2 km from the ground projection of the drone for different drone transmit power with simulations. Figure 3(b) shows the mean local delay of a D2D user against its distance from the ground projection of the drone with different transmit power of the drone and simulations. Figure 3(c) illustrates the network coverage probability after time slot T_n for different transmit power of the drone with simulations.

From Figures 3(a) and 3(b), we can see that our analytical results for link performance provide a good approximation to the simulation. The small gap between them comes from two reasons: (i) ignorance of the inhomogeneity of the active TXs inside the D2D user's sensitivity region, and (ii) ignorance of the correlation between the locations of active D2D TXs across different time slots, as discussed in Remark 1. From the figures, we can see that the gap between the simulation and the analytical results is small with a maximum relative absolute error less than 2.2% which validates the assumption made in Remark 1. Figure 3(c) also shows that the approximation we made in Remark 2 in the analysis of the network performance provides good accuracy. We only show the numerical results in the later subsections, since the numerical results are verified by comparison with the simulation.

Insights: Figure 3(a) shows that the increase in the drone transmit power improves the link coverage probability of the cell edge user. With a higher transmit power of the drone, the link coverage probability of the cell edge user approaches 1 faster. From Figure 3(b), we can see that the benefit of increasing transmit power of the drone is more significant for the D2D users further away from the ground projection of the drone than for the ones closer to the ground projection of the drone. Figure 3(c) illustrates that a higher drone transmit power provides a higher network coverage probability. With a higher transmit power of the drone, the network coverage probability approaches 1 using less time slots. This is because that more D2D users successfully receive the message after the first time slot T_0 if the drone broadcasts with a higher transmit power. Therefore, there are more active D2D users which multicast the message from the second time slot T_1 onwards and the message spreads over the network region more quickly.

C. IMPACT OF DRONE HEIGHT

In Figure 4(a), Figure 4(b) and Figure 4(c), we investigate the effect of deployment height of the drone on the link coverage probability at the cell edge user, the mean local delay of a D2D user and the network coverage probability after time slot T_n respectively.

Insights: Figure 4(a) shows the link coverage probability after time slot T_n at the cell edge user located at 2 km from the ground projection of the drone for different drone height. From this figure, we can see that the link coverage probability of the cell edge user after certain time slots is higher if the drone is deployed at a higher altitude at the first time slot T_0. With a higher altitude of the drone, the link coverage probability of the cell edge user approaches 1 after less time slots. Figure 4(b) plots the mean local delay of a D2D user against its distance from the ground projection of the drone

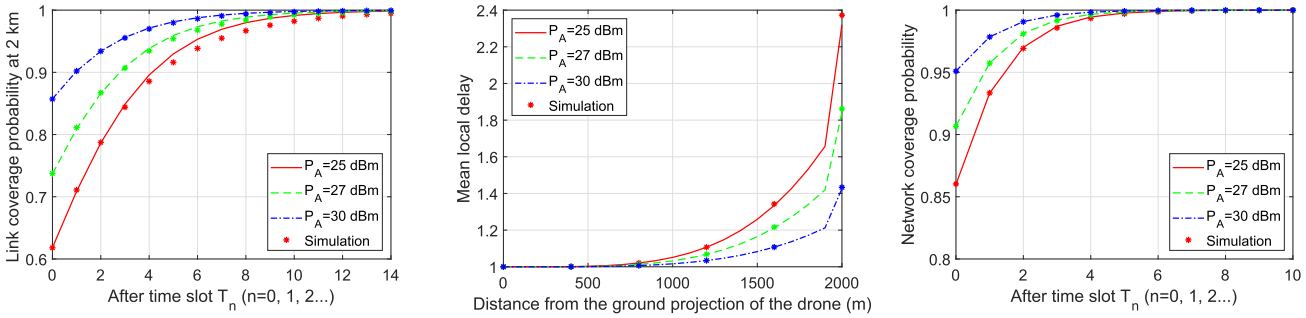

(a) Link coverage probability after time slot T_n at the cell edge user located at 2 km from the ground projection of the drone.

(b) Mean local delay of a D2D user versus its distance from the ground projection of the drone.

(c) Network coverage probability after time slot T_n.

FIGURE 3. Link performance and network performance with different transmit power of the drone and simulations.

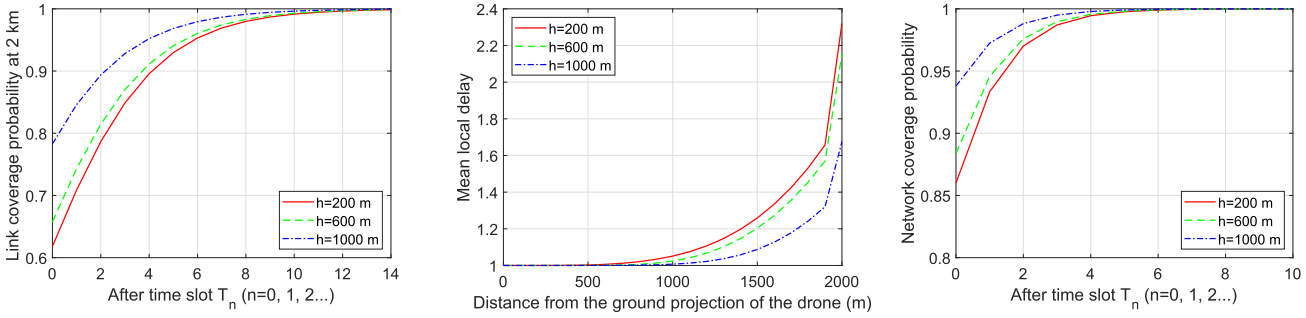

(a) Link coverage probability after time slot T_n at the cell edge user located at 2 km from the ground projection of the drone.

(b) Mean local delay of a D2D user versus its distance from the ground projection of the drone.

(c) Network coverage probability after time slot T_n.

FIGURE 4. Link performance and network performance with different height of the drone.

with different height of the drone. The figure shows that the increase of the deployment height of the drone decreases the mean local delay more significantly for the D2D users further away from the ground projection of the drone than for the ones closer to the ground projection of the drone. Although the signal propagates a longer distance as the height of the drone rises, there is higher probability that the link between the drone and the user around the cell edge is in LOS and thus experiences a lower path-loss.

Figure 4(c) illustrates the network coverage probability after time slot T_n for different deployment height of the drone. From the figure, we can find that a higher drone altitude provides a higher network coverage probability. The network coverage probability approaches 1 using less time slots when the drone is initially positioned at a higher height. This is because, if the drone is at a higher altitude, more D2D users around the cell edge receive the message and become active TX after the first time slot T_0 and the message spreads over the network region faster.

In order to further illustrate the advantage of using the drone in seeding the common emergency alert message, we consider a traditional D2D multicast multihop network where the common message is initially broadcasted by a D2D user located at the center of the network region on the ground. The numerical results for this special case can be obtained using our framework with some modifications. We find that the network coverage probability in this case reaches 88.75% after time slot T_{1000}. By comparison, from Figure 4(c), we can see that if the multihop multicasting is initiated by a drone deployed at $h = 200$ m, the network coverage probability is over 90% after only time slot T_1. This demonstrates the enormous advantage of exploiting the inherent mobility feature of drone communication, i.e., the drone can be deployed at a suitable height, to assist common information dissemination in D2D networks.

D. IMPACT OF D2D USER DENSITY

We study the impact of the density of D2D users on the link coverage probability at the cell edge user, the mean local delay of a D2D user and the network coverage probability after time slot T_n in Figure 5(a), Figure 5(b) and Figure 5(c) respectively.

Insights: Figure 5(a) illustrates the link coverage probability after time slot T_n at the cell edge user located at 2 km from the ground projection of the drone for different D2D user density. Figure 5(b) plots the mean local delay of a D2D user against its distance from the ground projection of the drone with various D2D user density. Figure 5(c) shows the

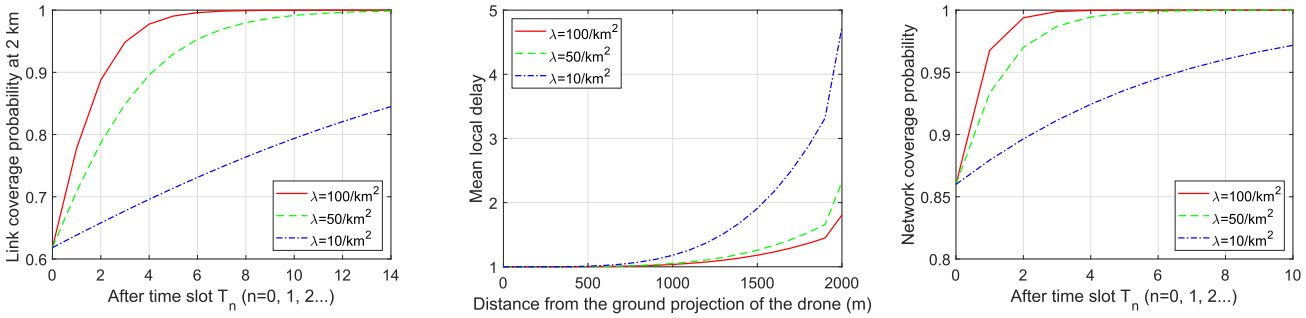

(a) Link coverage probability after time slot T_n at the cell edge user located at 2 km from the ground projection of the drone.

(b) Mean local delay of a D2D user versus its distance from the ground projection of the drone.

(c) Network coverage probability after time slot T_n.

FIGURE 5. Link performance and network performance with different D2D user density.

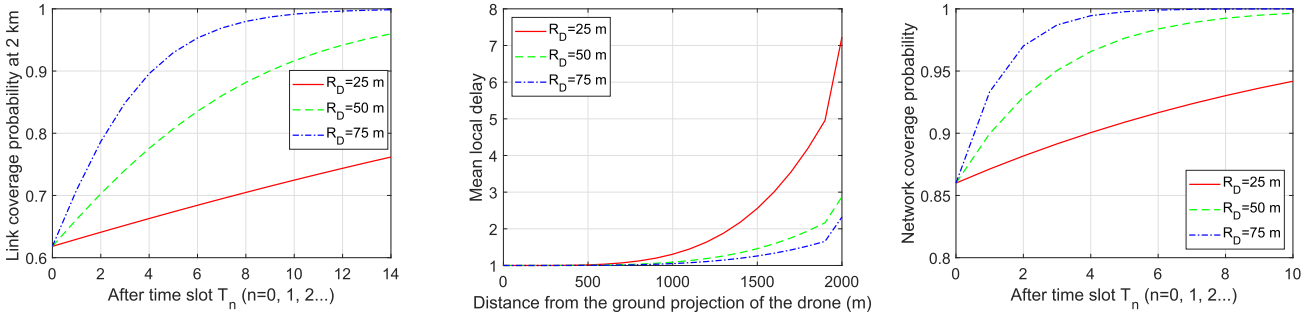

(a) Link coverage probability after time slot T_n at the cell edge user located at 2 km from the ground projection of the drone.

(b) Mean local delay of a D2D user versus its distance from the ground projection of the drone.

(c) Network coverage probability after time slot T_n.

FIGURE 6. Link performance and network performance with different D2D sensitivity radius.

network coverage probability after time slot T_n for different density of D2D users.

From Figure 5(a) and Figure 5(c), we can see that after a given number of time slots, the link coverage probability of the cell edge user and the network coverage probability are higher if the D2D user density is higher. Figure 5(b) demonstrates that the mean local delay of a D2D user at 2 km from the ground projection of the drone decreases from 4.736 time slots to 1.806 time slots, when the density of the D2D users increases from 10 per km^2 to 100 per km^2. With a higher density of D2D users, there are more D2D users in the cell that have received the message successfully and more active TXs located inside the D2D user's sensitivity region. So the message is delivered to the cell edge user within fewer time slots.

E. IMPACT OF D2D SENSITIVITY RADIUS

In Figure 6(a), Figure 6(b) and Figure 6(c), we evaluate the effect of the radius of D2D sensitivity region on the link coverage probability at the cell edge user after time slot T_n, the mean local delay of a D2D user and the network coverage probability after time slot T_n respectively.

Insights: Figures 6(a) and 6(c) show the link coverage probability at the cell edge user located at 2 km from the ground projection of the drone and the network coverage probability after time slot T_n for different radius of D2D sensitivity region. From these two figures, we can find that the link coverage probability of the cell edge user and the network coverage probability after a given number of time slots are higher if the D2D sensitivity region has a larger radius. This is because, there are more active TXs located inside the D2D user's sensitivity region if the radius is higher.

Figure 6(b) plots the mean local delay of a D2D user versus its distance from the ground projection of the drone with different radius of D2D sensitivity region. The figure shows that the increase of D2D sensitivity radius drops the mean local delay more significantly for the D2D users further away from the ground projection of the drone than for the ones closer to the ground projection of the drone. This is because, with a larger D2D sensitivity radius, the message multicasted by the active TXs located closer to the ground projection of the drone reaches the cell edge user within fewer hops.

VI. CONCLUSION

In this paper, we considered a drone-initiated D2D-aided multihop multicast network in public safety scenarios, where an emergency alert message is broadcasted by the drone and then multicasted by the D2D users which have successfully

received the message through multihop. A general analytical framework for link coverage probability and mean local delay for a D2D user was presented in terms of the link success probability, the network outage probability and the Laplace transform of the aggregate received signal power. An approximate and yet accurate analytical model was proposed for link success probability, network success probability and network coverage probability. The accuracy of the analytical results was verified by simulations. The results showed that the link performance and the network performance improve by raising the deployment altitude and the transmit power of the drone and increasing the density and the sensitivity radius of the D2D users. Future work can consider that the drone broadcasts the message above any random location in the network region.

APPENDIXES

APPENDIX A

PROOF OF THEOREM 1

From (2) and (4), we have

$$\begin{aligned}\mathbb{P}_s^0(X_i) &= \Pr(\mathsf{SNR}_0 > \gamma)\\ &= \Pr\left(\frac{P_{\mathrm{A}} G P L_a(\mathcal{Z})}{\sigma^2} > \gamma\right)\\ &= \Pr\left(G > \frac{\gamma\sigma^2}{P_{\mathrm{A}} P L_a(\mathcal{Z})}\right)\\ &= \Pr\left(G_{\mathrm{L}} > \frac{\gamma\sigma^2 z_i^{\alpha_{\mathrm{L}}}}{P_{\mathrm{A}}\eta_{\mathrm{L}}}\right) p_{\mathrm{L}} + \Pr\left(G_{\mathrm{N}} > \frac{\gamma\sigma^2 z_i^{\alpha_{\mathrm{N}}}}{P_{\mathrm{A}}\eta_{\mathrm{N}}}\right) p_{\mathrm{N}} \qquad (17a)\\ &= \sum_{i=0}^{m_{\mathrm{L}}-1} \frac{p_{\mathrm{L}}}{i!}\left(\frac{m_{\mathrm{L}}\gamma\sigma^2 z_i^{\alpha_{\mathrm{L}}}}{P_{\mathrm{A}}\eta_{\mathrm{L}}}\right)^i \exp\left(-\frac{m_{\mathrm{L}}\gamma\sigma^2 z_i^{\alpha_{\mathrm{L}}}}{P_{\mathrm{A}}\eta_{\mathrm{L}}}\right)\\ &\quad + \sum_{j=0}^{m_{\mathrm{N}}-1} \frac{p_{\mathrm{N}}}{j!}\left(\frac{m_{\mathrm{N}}\gamma\sigma^2 z_i^{\alpha_{\mathrm{N}}}}{P_{\mathrm{A}}\eta_{\mathrm{N}}}\right)^j \exp\left(-\frac{m_{\mathrm{N}}\gamma\sigma^2 z_i^{\alpha_{\mathrm{N}}}}{P_{\mathrm{A}}\eta_{\mathrm{N}}}\right), \qquad (17b)\end{aligned}$$

where (17a) comes from the fact that the aerial link between the drone and the D2D user has a probability p_{L} of being in LOS and a probability p_{N} of being in NLOS, respectively. Using the fact that the fading power gain for the LOS and NLOS aerial link, G_{L} and G_{N} follows Gamma distribution with parameters m_{L} and m_{N} respectively, (17b) can be worked out by the complementary cumulative distribution function of Gamma distribution and we can arrive at Theorem 1.

APPENDIX B

PROOF OF THEOREM 3

Following the definition of the Laplace transform, the Laplace transform of the aggregate received signal power distribution at the D2D user X_i is expressed as

$$\begin{aligned}\mathcal{L}_{P_i^n}(s) &= \mathbb{E}_P[\exp(-sP_i^n)]\\ &= \mathbb{E}_{\phi_{\text{active}}}\left[\exp\left(-s\sum_{X_j\in\phi_{\text{active}}} H_j \ell_j^{-\alpha_{\mathrm{T}}}\right)\right]\\ &= \mathbb{E}_{\phi_{\text{active}}}\left[\prod_{X_j\in\phi_{\text{active}}} \exp\left(-sH_j\ell_j^{-\alpha_{\mathrm{T}}}\right)\right]. \qquad (18)\end{aligned}$$

Conditioned on the location of the D2D user X_i, there are two possible cases for $\mathcal{L}_{P_i^n}(s)$. When $X_i \leqslant R_C - R_D$, the Laplace transform of the aggregate received signal power distribution at the D2D user equals to

$$\begin{aligned}\mathcal{L}_{P_i^n}(s) &= \exp\left(-\int_{-\pi}^{\pi}\int_0^{R_D} \mathbb{E}_H[1-\exp(-sH\ell^{-\alpha_{\mathrm{T}}})]\lambda_i^n \ell \mathrm{d}\ell\mathrm{d}\theta\right) \qquad (19a)\\ &= \exp\left(-\pi\lambda_i^n R_D^2 \mathbb{E}_H\left[1-\exp\left(-\frac{sH}{R_D^{\alpha_{\mathrm{T}}}}\right)\right]\right.\\ &\quad \left. -\pi\lambda_i^n \mathbb{E}_H\left[\Gamma\left(1-\frac{2}{\alpha_{\mathrm{T}}}, \frac{sH}{R_D^{\alpha_{\mathrm{T}}}}\right)\right]\right) \qquad (19b)\\ &= \exp\left(-\pi\lambda_i^n R_D^2 + \frac{2\pi\lambda_i^n R_D^{2+\alpha_{\mathrm{T}}}}{s(\alpha_{\mathrm{T}}+2)}\right.\\ &\quad \left. \times {}_2F_1\left(1, 1+\frac{2}{\alpha_{\mathrm{T}}}; 2+\frac{2}{\alpha_{\mathrm{T}}}; -\frac{R_D^{\alpha_{\mathrm{T}}}}{s}\right)\right), \qquad (19c)\end{aligned}$$

where (19a) follows the probability generating functional of PPP and $\Gamma(\cdot)$ in (19b) denotes the complete Gamma function. Using the fact that H follows an exponential distribution, (19c) can be worked out by taking the expectation over H. ${}_2F_1(\cdot,\cdot;\cdot;\cdot)$ is the Gaussian (or ordinary) hypergeometric function.

When $R_C - R_D < X_i \leqslant R_C$, the Laplace transform of the aggregate received signal power distribution at the D2D user is given as

$$\begin{aligned}&\mathcal{L}_{P_i^n}(s)\\ &= \underbrace{\exp\left(-\int_0^{R_C-X_i}\int_{-\pi}^{\pi} \mathbb{E}_H\left[1-\exp\left(-\frac{sH}{\ell^{\alpha_{\mathrm{T}}}}\right)\right]\lambda_i^n \ell \mathrm{d}\theta\mathrm{d}\ell\right)}_{A_1}\\ &\quad \times \underbrace{\exp\left(-\int_{R_C-X_i}^{R_D}\int_{-\omega}^{\omega} \mathbb{E}_H\left[1-\exp\left(-\frac{sH}{\ell^{\alpha_{\mathrm{T}}}}\right)\right]\lambda_i^n \ell \mathrm{d}\theta\mathrm{d}\ell\right)}_{A_2}, \qquad (20)\end{aligned}$$

where the first term A_1 corresponds to the D2D active TXs falling at the ring with radius from 0 to $R_C - X_i$ and the second term A_2 corresponds to the D2D active TXs falling at the arc with angle 2ω and radius from $R_C - X_i$ to R_D as shown in Figure 7. Using cosine rule, $\omega = \operatorname{arcsec}\left(\frac{2\ell X_i}{\ell^2 + X_i^2 - R_C^2}\right)$. A_1 can be evaluated follow similar step as in (19c).

The second term A_2 is evaluated as

$$\begin{aligned}A_2 &= \exp\left(-\int_{R_C-X_i}^{R_D} 2\mathbb{E}_H[1-\exp(-sH\ell^{-\alpha_{\mathrm{T}}})]\lambda_i^n \ell\omega \mathrm{d}\ell\right)\\ &= \exp\left(-\int_{R_C-X_i}^{R_D} \frac{2s\lambda_i^n \ell\omega}{\ell^{\alpha_{\mathrm{T}}}+s}\mathrm{d}\ell\right), \qquad (21)\end{aligned}$$

where (21) comes from the fact that H follows exponential distribution with unit mean.

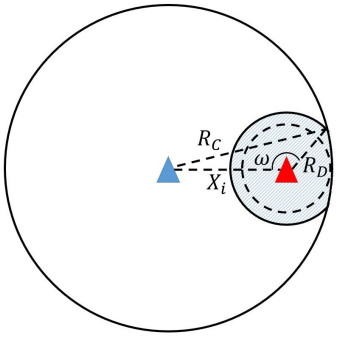

FIGURE 7. Illustration of the bounded sensitivity region (shaded blue) of a D2D user (red triangle) located more than $R_C - R_D$ m away from the ground projection of the drone (blue triangle).

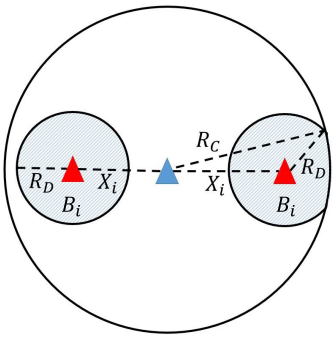

FIGURE 8. Illustration of the bounded sensitivity regions of D2D user X_i.

Combining (19c), (20) and (21), we can arrive at Theorem 3.

APPENDIX C
PROOF OF LEMMA 1

Following the simplification assumption we made in Remark 2, the approximated link success probability for D2D user X_i at T_n for $n = 1, 2, 3 \ldots$ is expressed as

$$\widetilde{\mathbb{P}}_s^n(X_i) = 1 - \Pr(N(B_i) = 0) = 1 - \exp(-\lambda_i^n |B_i|), \quad (22)$$

where B_i is the bounded sensitivity region of D2D user X_i and $N(B_i)$ is a random counting measure that counts the number of points falling in B_i. For a homogeneous PPP, $N(B_i)$ has a special case as shown above. $|\cdot|$ denotes the Lebesgue measure, which is the area in a two-dimensional case.

Therefore, the key is to compute the area of the bounded sensitivity region of D2D user X_i, $|B_i|$. From Figure 8, we can see that there are two different cases based on the location of the D2D user X_i. When $X_i \leqslant R_C - R_D$, the bounded sensitivity region B_i forms a circle with radius R_D. Hence, its area equals to

$$|B_i| = \pi R_D^2. \quad (23)$$

When $R_C - R_D < X_i \leqslant R_C$, the bounded sensitivity region B_i becomes an irregular ellipse. Using trigonometry, we can find that the area of B_i can be evaluated as

$$\begin{aligned} |B_i| = {} & R_C^2 \arccos\left(\frac{R_C^2 + X_i^2 - R_D^2}{2X_i R_C}\right) \\ & - \frac{1}{2}\sqrt{-R_C^4 - R_D^4 - X_i^4 + 2R_C^2 X_i^2 + 2R_D^2 X_i^2 + 2R_C^2 R_D^2} \\ & - R_D^2 \left(\arccos\left(\frac{R_C^2 - X_i^2 - R_D^2}{2X_i R_D}\right) - \pi\right). \end{aligned} \quad (24)$$

Substituting (23) and (24) into (22), we can arrive at Lemma 1.

REFERENCES

[1] Y. Zeng, Q. Wu, and R. Zhang, "Accessing from the sky: A tutorial on UAV communications for 5G and beyond," *Proc. IEEE*, vol. 107, no. 12, pp. 2327–2375, Dec. 2019.

[2] I. Bor-Yaliniz and H. Yanikomeroglu, "The new frontier in RAN heterogeneity: Multi-tier drone-cells," *IEEE Commun. Mag.*, vol. 54, no. 11, pp. 48–55, Nov. 2016.

[3] M. Mozaffari, W. Saad, M. Bennis, Y. N. Nam, and M. Debbah, "A tutorial on UAVs for wireless networks: Applications, challenges and open problems," *IEEE Commun. Surveys Tuts.*, vol. 21, no. 3, pp. 2334–2360, 3rd Quart., 2019.

[4] A. Asadi, Q. Wang, and V. Mancuso, "A survey on device-to-device communication in cellular networks," *IEEE Commun. Surveys Tuts.*, vol. 16, no. 4, pp. 1801–1819, 4th Quart., 2014.

[5] Y. Zeng, R. Zhang, and T. J. Lim, "Wireless communications with unmanned aerial vehicles: Opportunities and challenges," *IEEE Commun. Mag.*, vol. 54, no. 5, pp. 36–42, May 2016.

[6] V. Sharma, I. You, and R. Kumar, "Energy efficient data dissemination in multi-UAV coordinated wireless sensor networks," *Mobile Inf. Syst.*, vol. 2016, pp. 1–13, May 2016.

[7] X. Fan, C. Huang, B. Fu, S. Wen, and X. Chen, "UAV-assisted data dissemination in delay-constrained VANETs," *Mobile Inf. Syst.*, vol. 2018, pp. 1–12, Oct. 2018.

[8] F. Zeng, R. Zhang, X. Cheng, and L. Yang, "UAV-assisted data dissemination scheduling in VANETs," in *Proc. IEEE ICC*, May 2018, pp. 1–6.

[9] H. He, S. Zhang, Y. Zeng, and R. Zhang, "Joint altitude and beamwidth optimization for UAV-enabled multiuser communications," *IEEE Commun. Lett.*, vol. 22, no. 2, pp. 344–347, Feb. 2018.

[10] Q. Wu, Y. Zeng, and R. Zhang, "Joint trajectory and communication design for multi-UAV enabled wireless networks," *IEEE Trans. Wireless Commun.*, vol. 17, no. 3, pp. 2109–2121, Mar. 2018.

[11] A. A. Nasir, H. D. Tuan, T. Q. Duong, and H. V. Poor, "UAV-enabled communication using NOMA," *IEEE Trans. Commun.*, vol. 67, no. 7, pp. 5126–5138, Jul. 2019.

[12] M. Alzenad, A. El-Keyi, F. Lagum, and H. Yanikomeroglu, "3-D placement of an unmanned aerial vehicle base station (UAV-BS) for energy-efficient maximal coverage," *IEEE Wireless Commun. Lett.*, vol. 6, no. 4, pp. 434–437, Aug. 2017.

[13] A. Fotouhi, M. Ding, and M. Hassan, "Flying drone base stations for macro hotspots," *IEEE Access*, vol. 6, pp. 19530–19539, Apr. 2018.

[14] A. M. Hayajneh, S. A. R. Zaidi, D. C. Mclernon, M. D. Renzo, and M. Ghogho, "Performance analysis of UAV enabled disaster recovery networks: A stochastic geometric framework based on cluster processes," *IEEE Access*, vol. 6, pp. 26215–26230, Jun. 2018.

[15] M. Mozaffari, W. Saad, M. Bennis, and M. Debbah, "Unmanned aerial vehicle with underlaid device-to-device communications: Performance and tradeoffs," *IEEE Trans. Wireless Commun.*, vol. 15, no. 6, pp. 3949–3963, Jun. 2016.

[16] V. V. Chetlur and H. S. Dhillon, "Downlink coverage analysis for a finite 3-D wireless network of unmanned aerial vehicles," *IEEE Trans. Commun.*, vol. 65, no. 10, pp. 4543–4558, Oct. 2017.

[17] M. M. Azari, Y. Murillo, O. Amin, F. Rosas, M.-S. Alouini, and S. Pollin, "Coverage maximization for a poisson field of drone cells," in *Proc. IEEE PIMRC*, Oct. 2017, pp. 1–6.

[18] C. Liu, M. Ding, C. Ma, Q. Li, Z. Lin, and Y.-C. Liang, "Performance analysis for practical unmanned aerial vehicle networks with LoS/NLoS transmissions," in *Proc. IEEE ICC Workshops*, May 2018, pp. 1–6.

[19] B. Galkin, J. Kibilda, and L. A. DaSilva, "Coverage analysis for low-altitude UAV networks in urban environments," in *Proc. IEEE Globecom*, Dec. 2017, pp. 1–6.
[20] M. Alzenad and H. Yanikomeroglu, "Coverage and rate analysis for unmanned aerial vehicle base stations with LoS/NLoS propagation," in *Proc. IEEE Globecom Workshop*, Dec. 2018, pp. 1–7.
[21] R. Fan, J. Cui, S. Jin, K. Yang, and J. An, "Optimal node placement and resource allocation for UAV relaying network," *IEEE Commun. Lett.*, vol. 22, no. 4, pp. 808–811, Apr. 2018.
[22] S. Zhang, H. Zhang, Q. He, K. Bian, and L. Song, "Joint trajectory and power optimization for UAV relay networks," *IEEE Commun. Lett.*, vol. 22, no. 1, pp. 161–164, Jan. 2018.
[23] C. Pan, H. Ren, Y. Deng, M. Elkashlan, and A. Nallanathan, "Joint blocklength and location optimization for URLLC-enabled UAV relay systems," *IEEE Commun. Lett.*, vol. 23, no. 3, pp. 498–501, Mar. 2019.
[24] Y. Xu, X. Li, and J. Zhang, "Device-to-device content delivery in cellular networks: Multicast or unicast," *IEEE Trans. Veh. Technol.*, vol. 67, no. 5, pp. 4401–4414, May 2018.
[25] H. Meshgi, D. Zhao, and R. Zheng, "Optimal resource allocation in multicast device-to-device communications underlaying LTE networks," *IEEE Trans. Veh. Technol.*, vol. 66, no. 9, pp. 8357–8371, Sep. 2017.
[26] X. Lin, R. Ratasuk, A. Ghosh, and J. G. Andrews, "Modeling, analysis and optimization of multicast device-to-device transmissions," *IEEE Trans. Wireless Commun.*, vol. 13, no. 8, pp. 4346–4359, Aug. 2014.
[27] A. Khisti, U. Erez, and G. W. Wornell, "Fundamental limits and scaling behavior of cooperative multicasting in wireless networks," *IEEE Trans. Inf. Theory*, vol. 52, no. 6, pp. 2762–2770, Jun. 2006.
[28] T. V. Santana, R. Combes, and M. Kobayashi, "Device-to-device aided multicasting," in *Proc. IEEE ISIT*, Jun. 2018, pp. 771–775.
[29] C.-H. Liu and J. G. Andrews, "Multicast outage probability and transmission capacity of multihop wireless networks," *IEEE Trans. Inf. Theory*, vol. 57, no. 7, pp. 4344–4358, Jul. 2011.
[30] A. A. Khuwaja, Y. Chen, N. Zhao, M.-S. Alouini, and P. Dobbins, "A survey of channel modeling for UAV communications," *IEEE Commun. Surveys Tuts.*, vol. 20, no. 4, pp. 2804–2821, 4th Quart., 2018.
[31] A. Al-Hourani, S. Kandeepan, and A. Jamalipour, "Modeling air-to-ground path loss for low altitude platforms in urban environments," in *Proc. IEEE Globecom*, Dec. 2014, pp. 2898–2904.
[32] X. Zhou, S. Durrani, J. Guo, and H. Yanikomeroglu, "Underlay drone cell for temporary events: Impact of drone height and aerial channel environments," *IEEE Internet Things J.*, vol. 6, no. 2, pp. 1704–1718, Apr. 2019.
[33] S. Seong, I. Sohn, S. Choi, and K. B. Lee, "Distributed synchronization algorithm for infrastructure-less public safety networks," *J. Commun. Netw.*, vol. 20, no. 3, pp. 316–324, Jun. 2018.
[34] D. T. Roche, B. Champagne, I. Psaromiligkos, and B. Pelletier, "On the use of distributed synchronization in 5G device-to-device networks," in *Proc. IEEE ICC*, May 2017, pp. 1–7.
[35] W. Sun, M. R. Gholami, E. G. Ström, and F. Brännstrom, "Distributed clock synchronization with application of D2D communication without infrastructure," in *Proc. IEEE Globecom Workshop*, Dec. 2013, pp. 561–566.
[36] Y.-C. Ko, M. S. Alouini, and M. K. Simon, "Outage probability of diversity systems over generalized fading channels," *IEEE Trans. Commun.*, vol. 48, no. 11, pp. 1783–1787, Nov. 2000.
[37] X. Zhou, J. Guo, S. Durrani, and M. Di Renzo, "Power beacon-assisted millimeter wave ad hoc networks," *IEEE Trans. Commun.*, vol. 66, no. 2, pp. 830–844, Feb. 2018.
[38] I. Bor-Yaliniz, A. El-Keyi, and H. Yanikomeroglu, "Efficient 3-D placement of an aerial base station in next generation cellular networks," in *Proc. IEEE ICC*, May 2016, pp. 1–5.
[39] M. Mozaffari, W. Saad, M. Bennis, and M. Debbah, "Mobile unmanned aerial vehicles (UAVs) for energy-efficient Internet of Things communications," *IEEE Trans. Wireless Commun.*, vol. 16, no. 11, pp. 7574–7589, Nov. 2017.

XIAOHUI ZHOU (Student Member, IEEE) received the B.Eng. degree (Hons.) in electronics and communications and mechatronics engineering and the Ph.D. degree in telecommunications engineering from The Australian National University (ANU), Canberra, Australia, in 2014 and 2019, respectively. Her research interests include drone communications, millimeter wave communications, wireless information and power transfer, stochastic geometry, and fifth-generation wireless networks. She was a recipient of ANU University Research Scholarship.

SALMAN DURRANI (Senior Member, IEEE) received the B.Sc. degree (Hons.) in electrical engineering from the University of Engineering and Technology, Lahore, Pakistan, in 2000, and the Ph.D. degree in electrical engineering from the University of Queensland, Brisbane, Australia, in December 2004. He has been with The Australian National University, Canberra, Australia, since 2005, where he is currently an Associate Professor with the Research School of Electrical, Energy and Materials Engineering, College of Engineering & Computer Science. He has coauthored more than 140 publications to date in refereed international journals and conferences. His research interests include wireless information and power transfer, energy-harvesting-enabled wireless communications, drone communications, machine-to-machine and device-to-device communication, stochastic geometry modeling of finite area networks, and synchronization in communication systems.

Dr. Durrani is a member of Engineers Australia, and a Senior Fellow of The Higher Education Academy, U.K. He was a recipient of the 2016 IEEE ComSoc Asia Pacific Outstanding Paper Award. He was the Chair of the ACT Chapter of the IEEE Signal Processing and Communications Societies from 2015 to 2016. He was awarded the Special Commendation in the 2012 ANU VC Award for Excellence in Education, the 2018 ANU VC Award for Excellence in Supervision, and the 2019 ACGR Award for Excellence in Graduate Research Supervision. He currently serves as an Editor for the IEEE TRANSACTIONS ON COMMUNICATIONS.

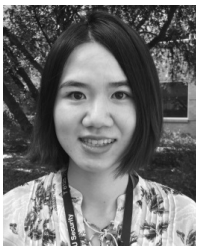

JING GUO (Member, IEEE) received the B.Sc. degrees (Hons.) in electronics and telecommunications engineering from The Australian National University (ANU), Canberra, Australia, and the Beijing Institute of Technology (BIT), China, in 2012, and the Ph.D. degree in telecommunications engineering from ANU in 2016. From 2016 to 2018, she was employed as a Postdoctoral Research Fellow with the Research School of Electrical, Energy and Materials Engineering, ANU. She is currently an Associate Professor with the School of Information and Electronics, BIT. Her research interest include in the field of wireless communications, including drone communications, machine-to-machine communications, and the application of stochastic geometry to wireless networks.